J Mater Sci (2009) 44:4754–4757
DOI 10.1007/s10853-009-3722-2

LETTER

Charge compensation in an irradiation-induced phase of δ-$Sc_4Zr_3O_{12}$

Michael W. Blair · Mark R. Levy · Robin W. Grimes · Blas P. Uberuaga · Chao Jiang · James A. Valdez · Josh J. Williams · Ming Tang · Christopher R. Stanek · Kurt E. Sickafus

Received: 29 May 2009 / Accepted: 2 July 2009 / Published online: 19 July 2009

Robust materials that are durable under irradiation are needed by a resurgent nuclear industry, and oxide ceramics are leading candidates for a number of nuclear applications, such as the storage of nuclear waste [1]. The delta (δ) phase of $Sc_4Zr_3O_{12}$ is an example of an oxide that has recently been shown to have excellent radiation tolerance/amorphization resistance [2, 3]. It has been proposed that the origin of the pronounced radiation tolerance in such materials is linked to crystal structure characteristics [3]. The structure of δ-$Sc_4Zr_3O_{12}$ is similar to that of fluorite (CaF_2), but with rhombohedral (not cubic) symmetry (space group $R\bar{3}$ [4]). Ion irradiation damage experiments on δ-$Sc_4Zr_3O_{12}$ using 300 keV Kr^{2+} ions, have revealed an order-to-disorder (O-D) phase transformation from an ordered δ-phase to a disordered fluorite structure at low ion dose [2]. This O-D transformation is similar to that observed in other fluorite derivative oxides, especially pyrochlore compounds [5]. However, in δ-$Sc_4Zr_3O_{12}$ at high ion dose, a surprising second transformation, a disorder-to-order (D-O) transformation, was observed [6]. This D-O transformation was shown to involve a structural rearrangement from a disordered fluorite to an ordered bixbyite structure [6]. Sickafus et al. [7] found that the irradiation-induced bixbyite phase contained a high concentration of Zr. The Sc:Zr ratio in the bixbyite phase was found to be 4:3, just as it is in the δ-phase (to within the error of the experimental measurements). This is unexpected because bixbyites are usually sesquioxide compositions with a trivalent cation. This said, we would propose to write the composition of the irradiation-induced bixbyite as $(Sc_{4/7}Zr_{3/7})_2O_3$, where the compound is made solely from 3^+ cations. It is, however, well known that Zr strongly desires a 4+ valence. Thus, the bixbyite formula, $(Sc_{4/7}Zr_{3/7})_2O_3$, runs counter to intuition. Here we attempt to identify the charge compensation mechanism for incorporation of excess Zr in a Sc–Zr–O bixbyite.

As mentioned previously, one of the possible charge compensation mechanisms for Zr incorporation in a Sc–Zr–O bixbyite involves Zr^{3+}. This ion is a paramagnetic species, so we used EPR spectroscopy to determine the relative abundance of Zr^{3+} in both a pristine δ-$Sc_4Zr_3O_{12}$ sample and in an irradiated δ-$Sc_4Zr_3O_{12}$ sample that contains the bixbyite phase. Figure 1 shows mass-corrected, first-derivative EPR spectra, measured at 5 K, for both pristine and irradiated δ-$Sc_4Zr_3O_{12}$. Both samples display a weak signal (approximately 10^{12} spins/g) with a g-value of approximately 2.0027, calibrated against DPPH. This is close to the free electron value of 2.00238. Figure 1 also shows an EPR spectrum obtained from a zirconia sample that was annealed in a reducing environment to produce a nominal composition of $\sim ZrO_{1.98}$ containing Zr^{3+} ions [2]. The EPR spectrum from this reduced compound is remarkably similar to that from the ion-irradiated δ-$Sc_4Zr_3O_{12}$ sample containing the bixbyite phase. Similar studies [8, 9] on reduced ZrO_2 samples have associated

M. W. Blair (✉)
Earth and Environmental Science Division, Los Alamos National Laboratory, Los Alamos, NM 87545, USA
e-mail: mblair@lanl.gov

M. R. Levy
British Energy plc., Barnett Way, Barnwood, Gloucester GL4 3RS, UK

R. W. Grimes
Department of Materials, Imperial College London, London SW7 2AZ, UK

B. P. Uberuaga · C. Jiang · J. A. Valdez · J. J. Williams · M. Tang · C. R. Stanek · K. E. Sickafus
Materials Science and Technology Division, Los Alamos National Laboratory, Los Alamos, NM 87545, USA

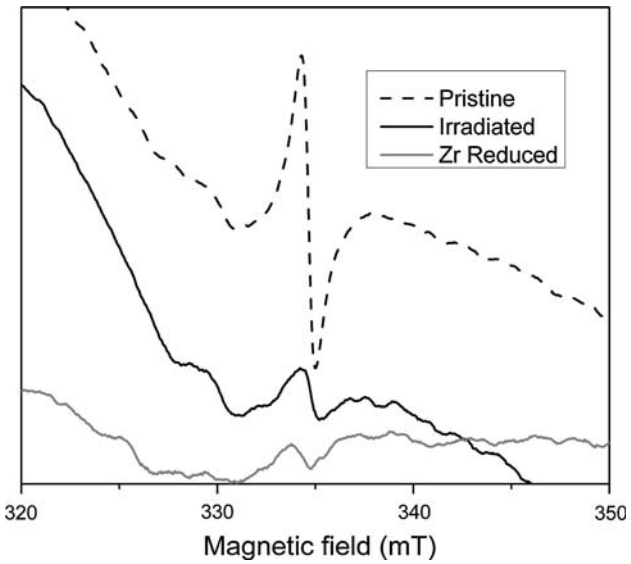

Fig. 1 EPR spectra measured at 5 K of pristine δ-$Sc_4Zr_3O_{12}$, irradiated δ-$Sc_4Zr_3O_{12}$, and a reduced Zr sample. The spectra were measured with a Bruker EleXsys E500 X-band spectrometer

Zr^{3+} ions with EPR signals ranging from $g = 1.953$ to 1.981, but Occhiuzzi et al. [10] have identified these signals as Cr impurities. These studies [8–10] also identified EPR signals with g values and linewidths similar to our EPR signals as F^+ centers, but they did not use samples containing nuclei with nuclear moments. However, in our δ-$Sc_4Zr_3O_{12}$ samples, we do not detect hyperfine splitting due to Sc nuclei ($I = 7/2$ with 100% abundance). Since our samples contain large concentrations of Sc, the lack of hyperfine splitting makes the presence of F^+ centers unlikely. All of our samples (i.e., pristine and irradiated δ-$Sc_4Zr_3O_{12}$ and reduced $ZrO_{1.98}$), contain tetravalent cation, Zr^{4+}; but Zr^{4+} is EPR silent. Thus, the most likely origin of the EPR signal in our measurements is due to the presence of Zr^{3+}. Although the occurrence of Zr^{3+} is rarely identified, Abraham et al. [11] found Zr^{3+} in monzanite-structured orthophosphates at lower g values than in the current. The addition of the tetragonal distortion in the orthophosphates accounts for the anisotropy of the g tensor and the deviation of the g values from that of the free electron.

At first glance, a comparison of the EPR signal intensities in Fig. 1 suggests that irradiation decreases the amount of Zr^{3+}. On the contrary, an analysis of the EPR line-shapes tells a different story. We were able to fit the EPR signal from the pristine δ-$Sc_4Zr_3O_{12}$ sample to a Lorentzian line-shape. This shape would be expected for a moderately low concentration of Zr^{3+} ions [12]. However, a similar analysis of the EPR signal from the irradiated δ-$Sc_4Zr_3O_{12}$ sample revealed that this signal is best described by a Dysonian line-shape. This shape is typical of EPR signals from metals [13] or samples with high concentrations of the detected ions [14] (i.e., with small nearest or second nearest neighbor separation distances between Zr^{3+} ions). In order to characterize the metallic nature of the EPR signals more fully, we calculated the dispersion-to-absorption ratio, α. Specifically, we measured the intensity of the dispersion signal (the low-field side of the resonance) and compared this to the intensity of the absorption signal (the high-field side of the resonance). For the pristine δ-$Sc_4Zr_3O_{12}$ sample, we obtained an α value of 1.11. This indicates that the measured EPR resonance is, indeed, Lorentzian, as previously concluded. The irradiated δ-$Sc_4Zr_3O_{12}$ sample yielded an α value of 1.71, which implies a larger Zr^{3+} concentration but is still less than the limit for a mobile, conduction-like spin [15]. Considering that any deviation in shape from the pristine sample most likely arises from the bixbyite phase (which makes up less than 0.01% of the sample by volume), the Zr^{3+} concentration must be very high. We further analyzed the EPR signals by normalizing the intensities for both the pristine and irradiated samples, then subtracted the irradiated resonance from the pristine resonance to yield the shape of the EPR signal that arises from the bixbyite phase. The α value for the resulting resonance is 3.76. This indicates a mobile, conduction-like spin (similar to signals from metals) and a very high concentration of Zr^{3+} ions [14].

To help interpret the experimental results, we performed density functional theory (DFT) calculations, using the VASP code [16–19], with PAW pseudopotentials [20, 21], a generalized gradient approximation (GGA) exchange–correlation functional, and a $2 \times 2 \times 2$ k-point sampling of the Monkhorst-Pack type [22]. Specifically, we examined Sc_2O_3 systems with varying concentrations of Zr ions. For the Zr-bearing calculations we discuss here, the Sc:Zr ratio was 3.85:3, as close to the δ-$Sc_4Zr_3O_{12}$ stoichiometry as we could accommodate in our simulation cell (containing a total of 80 atoms). In this calculation, the Zr and Sc atoms were randomly distributed on M sites in an M_2O_3 sesquioxide bixbyite lattice.

Figure 2 shows the band structure of Sc_2O_3 with and without Zr, as calculated with DFT. We find a bandgap of 3.74 eV for Sc_2O_3. This is lower than the experimental value of 6.3 eV [23], but this discrepancy is typical of DFT within the GGA approximation. In the Zr-loaded simulation cell, a band of filled electronic states is created just below the conduction band, and the bandgap is reduced to just 0.2 eV. This is consistent with the EPR results that Zr-bearing Sc_2O_3 is metallic. Furthermore, the character of the gap changes: Sc_2O_3 has a direct bandgap, but in the Zr-loaded cell, the bandgap becomes indirect. In order to further understand this change in the electronic structure, we have performed a Bader analysis [24] of the ionic charges in the material. Care must be taken when carrying out such an analysis, as assigning charges to ions is not meaningful for a metallic system. We find that the net

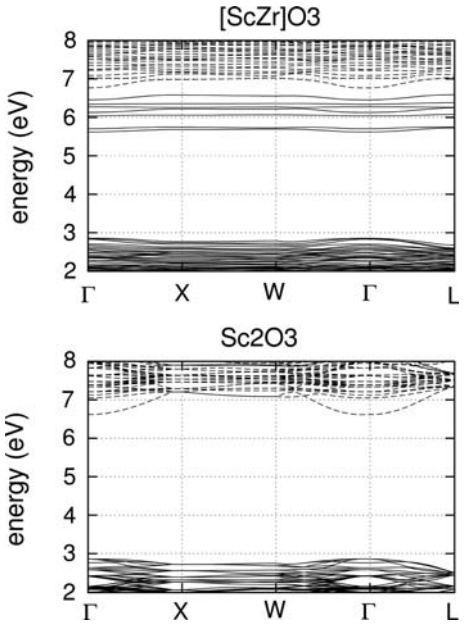

Fig. 2 Difference in electronic charge on ions in pristine Sc_2O_3 and Zr-loaded Sc_2O_3, as calculated with DFT and Bader analysis

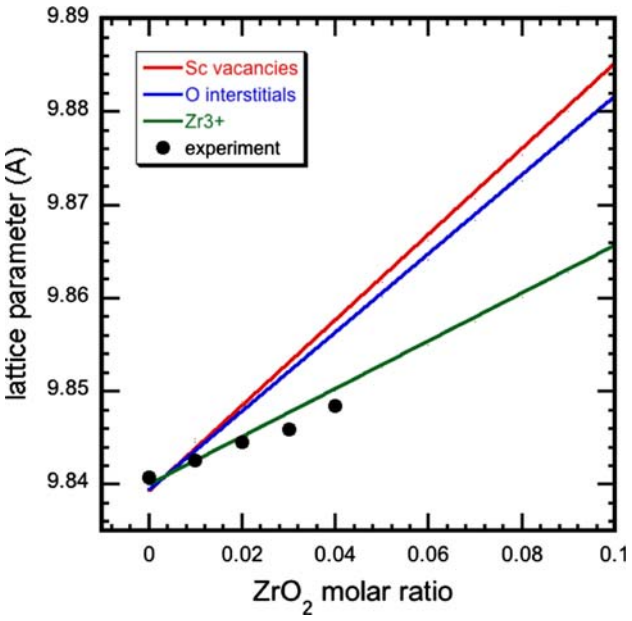

Fig. 3 Predicted changes in lattice parameter in Sc_2O_3 as a function of Zr content for three different defect incorporation (charge compensation) mechanisms, compared with experimentally observed lattice parameter changes

charge on the Sc ions is about +2.5, while that on the Zr ions varies between +2 and +2.5. This suggests that the Zr ions can accommodate charge states very similar to Sc. We have also calculated the elastic constants of the Zr-doped Sc_2O_3 using the same methods as Jiang et al. [25], to ensure that the structural stability of the compound within our calculations is not an artifact of the boundary conditions. We find the material to be mechanically stable, with $c_{11} = 281$ GPa, $c_{12} = 120$ GPa, and $c_{44} = 80$ GPa. These elastic constants clearly satisfy the mechanical stability criteria of $c_{11} > c_{12}$, $c_{44} > 0$ and $c_{11} + 2c_{12} > 0$.

Next, we performed molecular statics simulations using Buckingham potentials [26, 27] in order to predict defect volumes associated with the possible mechanisms by which Zr can be substituted onto Sc sites in Sc_2O_3 bixbyite. There are three simple solution mechanisms, namely: (1) Zr^{4+} ions at Sc sites charge compensated by Sc vacancies; (2) Zr^{4+} ions at Sc sites charge compensated by O interstitial ions; and (3) electronic structure alteration so that Zr ions on Sc sites assume 3+ charge states (i.e., Zr^{3+}). We related the respective defect volumes with predicted changes in lattice parameter as in Patel et al. [28]. Figure 3 shows the predicted lattice parameter variation with Zr content for the three charge compensation mechanisms described above. It is clear from Fig. 3 that all three mechanisms result in a positive defect volume, and thus an expansion of the lattice. The lattice expansion due to Zr^{3+} charge compensation is distinguishably less than that from the expansion associated with Sc vacancy or O interstitial formation.

It is interesting to consider the origins of lattice expansion for the three solution mechanisms considered. First, for the Sc vacancy and O interstitial mechanisms, we note that Zr^{4+} (VI) is smaller than Sc^{3+} (VI) (0.72 vs. 0.745 Å [29]). Therefore, the net expansions are related to the charge compensating defects; that is, O interstitial ions or Sc vacancies are causing the local expansion of the lattice. In addition, due to their charges, O interstitial and the Zr^{4+} substitutional ions are likely to bind (i.e., form clusters). This causes the local anion coordination around the Zr to increase, leading to an increase in cation size. On the other hand, for Zr^{3+}, there are no additional defects that contribute to lattice expansion or contraction. Furthermore, since Sc^{3+} and Zr^{3+} are isovalent, the only contribution to lattice expansion is due to the cationic radius of Zr^{3+} (VI) being larger than Sc^{3+} (VI) (though no value for Zr^{3+} (VI) is available in the literature).

Finally, using commercial powders of Sc_2O_3 and ZrO_2, we fabricated bulk ceramic alloys (in sintered pellet form) of scandia doped with zirconia, over the composition range 1–4 mol.% ZrO_2. These samples were sintered in a fully oxygenated (air) environment. We measured the lattice parameters of these alloys using X-ray diffraction, in order to compare experimental and predicted lattice parameters, the latter based on the charge compensation mechanisms described above. The measured (cubic) lattice parameters (a) are overlayed in Fig. 3 with our predicted lattice parameter trends. It is interesting that the best fit between measured and calculated lattice parameter trends is the

Zr^{3+} charge compensation model. Clearly, we cannot rule out Zr^{3+} as the dominant charge compensation mechanism in this alloy system.

Together, the experimental and theoretical results support the hypothesis that Zr is incorporated into the irradiated δ-$Sc_4Zr_3O_{12}$ in a reduced charge state and, as a result, the material is a much better electrical conductor. This is counter-intuitive, as Zr would normally be found in a +4 charge state. However, in the absence of interactions with the environment, where the oxygen content could change to accommodate various charge states of the cations, the Zr is able to exist in a more reduced charge state and effectively act as an n-type dopant. This leads to interesting possibilities for designing novel electronic materials. Similar effects could also be expected if the oxygen sublattice is doped with fluorine as it would act as an n-type dopant relative to oxygen. Indeed, DFT calculations suggest a similar creation of filled states just below the conduction band when half the oxygen sublattice is replaced with F. Finally, as discussed earlier, such a composition must be inherently metastable with a strong thermodynamic tendency to phase separate. That it did form under irradiation demonstrates that irradiation can be used to fabricate novel material compositions that are then kinetically trapped against decomposition.

Acknowledgements This work was sponsored by two programs from the U.S. Department of Energy (DOE), Office of Basic Energy Sciences (OBES), Division of Materials Sciences and Engineering.

References

1. Weber WJ, Ewing RC, Catlow CRA, de la Rubia TD, Hobbs LW, Kinoshita C, Matzke H, Motta AT, Nastasi M, Salje EKH, Vance ER, Zinkle SJ (1998) J Mater Res 13:1434
2. Valdez JA, Tang M, Sickafus KE (2006) Nucl Instr Methods Phys Res Sect B 250:148
3. Sickafus KE, Grimes RW, Valdez JA, Cleave A, Tang M, Ishimaru M, Corish SM, Stanek CR, Uberuaga BP (2007) Nat Mater 6:217
4. Hahn T (ed) (1983) International tables for crystallography, vol A: space-group symmetry. Reidel, Dordrecht, Netherlands
5. Lian J, Wang L, Chen J, Sun K, Ewing RC, Matt Farmer J, Boatner LA (2003) Acta Mater 51:1493
6. Ishimaru M, Hirotsu Y, Tang M, Valdez JA, Sickafus KE (2007) J Appl Phys 102:063532
7. Sickafus KE, Ishimaru M, Hirotsu Y, Usov IO, Valdez JA, Hosemann P, Johnson AL, Thao TT (2008) Nucl Instr Methods Phys Res B 266:2892
8. Morterra C, Giamello E, Orio L, Volante M (1990) J Phys Chem 94:3111
9. Qin Z, Xinping W, Tianxi C (2004) Appl Surf Sci 225:7
10. Occhiuzzi M, Cordischi D, Dragone R (2002) J Phys Chem B 106:12464
11. Abraham MM, Boatner LA, Ramey JO, Rappaz M (1984) J Chem Phys 81:5362
12. Poole CP (1983) Electron spin resonance: a comprehensive treatise on experimental techniques. Dover, Mineola, NY
13. Deisenhofer J, von Nidda HAK, Loidl A, Sampathkumaran EV (2003) Solid State Commun 125:327
14. Matsuishi S, Toda Y, Miyakawa M, Hayashi K, Kamiya T, Hirano M, Tanaka I, Hosono H (2003) Science 301:626
15. Kodera H (1970) J Phys Soc Jpn 28:89
16. Kresse G, Hafner J (1993) Phys Rev B 47:558
17. Kresse G, Hafner J (1994) Phys Rev B 49:14251
18. Kresse G, Furthmuller J (1996) Comput Mater Sci 6:15
19. Kresse G, Furthmuller J (1996) Phys Rev B (Condens Matter) 54:11169
20. Kresse G, Joubert D (1999) Phys Rev B (Condens Matter) 59:1758
21. Blochl PE (1994) Phys Rev B 50:17953
22. Monkhorst HJ, Pack JD (1976) Phys Rev B (Solid State) 13:5188
23. Emeline AV, Petrova SV, Ryabchuk VK, Serpone N (1998) Chem Mater 10:3484
24. Bader RFW (1190) Atoms in molecules—a quantum theory. Oxford University Press, Oxford
25. Jiang C, Srinivasan SG, Caro A, Maloy SA (2008) J Appl Phys 103:043502
26. Zacate MO, Minervini L, Bradfield DJ, Grimes RW, Sickafus KE (2000) Solid State Ionics 128:243
27. Levy MR, Steel BCH, Grimes RW (2004) Solid State Ionics 175:349
28. Patel AP, Levy MR, Grimes RW, Gaume RM, Feigelson RS, McClellan KJ, Stanek CR (2008) Appl Phys Lett 93:191902
29. Shannon RD (1976) Acta Crystallogr A A32:751